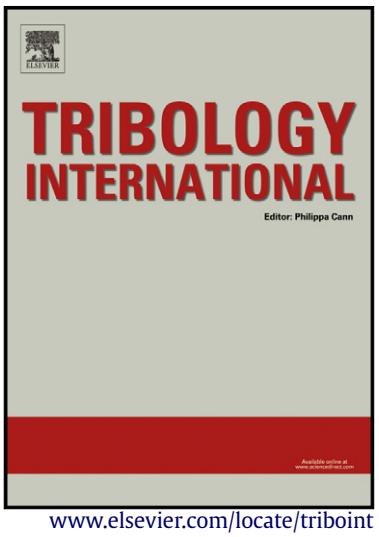

www.elsevier.com/locate/triboint

Study of the friction-induced vibration and contact mechanics of artificial hip joints

Ehsan Askari, Paulo Flores, Danè Dabirrahmani, Richard Appleyard

PII: S0301-679X(13)00303-4
DOI: http://dx.doi.org/10.1016/j.triboint.2013.09.006
Reference: JTRI3135

To appear in: *Tribology International*

Received date: 4 June 2013
Revised date: 9 August 2013
Accepted date: 6 September 2013

Cite this article as: Ehsan Askari, Paulo Flores, Danè Dabirrahmani, Richard Appleyard, Study of the friction-induced vibration and contact mechanics of artificial hip joints, *Tribology International,* http://dx.doi.org/10.1016/j.triboint.2013.09.006

Study of the friction-induced vibration and contact mechanics of artificial hip joints

Ehsan Askari [a, b *], Paulo Flores[b], Danè Dabirrahmani[a], Richard Appleyard[a]

[a] Australian School of Advanced Medicine, Macquarie University, Sydney
[b] Department of Mechanical Engineering, School of Engineering, University of Minho, Portugal

[*] Corresponding Author. Tel.: +61 416 073 601.
Email address: ehsanaskary@gmail.com (E. Askari).

Abstract

The main objective of this work is to study the effect of friction-induced vibration and contact mechanics on the maximum contact pressure and moment of artificial hip implants. For this purpose, a quasi-static analysis and a multibody dynamic approach are considered. It is shown that the multibody dynamic model is effective at predicting contact pressure distribution and moment of hip implants from both accuracy and time-consuming points of view. Finally, from the computational simulations performed, it can be observed that the friction-induced vibration influences the contact pressure and the moment in hip implants by introducing an oscillating behaviour in the system dynamics.

Keywords: Friction-induced vibration; Multibody dynamics; Contact mechanics; Artificial hip joints.

1. Introduction

It has been recognized by a good number of researchers that the computation of the pressure distribution and contact area of artificial hip joints during daily activities can play a key role in predicting prosthetic implant wear [1-4]. The Hertzian contact theory has been considered to evaluate the contact parameters, namely the maximum contact pressure and contact area by using the finite element method [1, 2]. Mak and his co-workers [1] studied the contact mechanics in ceramic-on-ceramic (CoC) hip implants subjected to micro-separation and it was shown that contact stress increased due to edge loading and it was mainly dependent on the magnitude of cup-liner separation, the radial clearance and the cup inclination angle [3, 4]. In fact, Hertzian contact theory can captured slope and curvature trends associated with contact patch geometry subjected to the applied load to predict the contact dimensions accurately in edge-loaded ceramic-on-ceramic hips [5]. Although the finite element analysis is a popular approach for investigating contact mechanics, discrete element technique has also been employed to predict contact pressure in hip joints [6]. As computational instability can occur when the contact nodes move near the edges of the contact elements, a contact smoothing approach by applying Gregory patches was suggested [7]. Moreover, the contributions of individual muscles and the effect of different gait patterns on hip contact forces are of interest, which can be determined by using optimization techniques and inverse dynamic analyses [8, 9]. In addition, contact stress and local temperature at the contact region of dry-sliding couples during wear tests of CoC femoral heads can experimentally be assessed by applying fluorescence microprobe spectroscopy [10]. The contact pressure distribution on the joint bearing surfaces can be used to determine the heat generated by friction and the volumetric wear of artificial hip joints [11, 12]. Artificial hip joint moment due to friction and the kinetics of hip implant components may cause prosthetic implant components to loosen, which is one of the main causes of failure of hip replacements. Knee and hip joints' moment values during stair up and sit-to-stand motions can be evaluated computationally [13]. The effect of both body-weight-support level and walking speed was investigated on mean peak internal joint moments at ankle, knee and hip [14]. However, in-vivo study of the friction moments acting on the hip demands more research in order to assess whether those findings could be generalised was carried out [15].

The hypothesis of the present study is that friction-induced vibration and stick/slip friction could affect maximum contact pressure and moment of artificial hip joints. This desideratum is achieved by developing a multibody dynamic model that is able to cope with the usual difficulties of

available models due to the presence of muscles, tendons and ligaments, proposing a simple dynamic body diagram of hip implant. For this purpose, a cross section through the interface of ball, stem and lateral soft and stiff tissues is considered to provide the free body diagram of the hip joint. In this approach, the ball is moving, while the cup is considered to be stationary. Furthermore, the multibody dynamic motion of the ball is formulated, taking the friction-induced vibration and the contact forces developed during the interaction with cup surface. In this study, the model utilises available information of forces acting at the ball centre, as well as angular rotation of the ball as functions of time during a normal walking cycle. Since the rotation angle of the femoral head and their first and second derivatives are known, the equation of angular momentum could be solved to compute external joint moment acting at the ball centre. The nonlinear governing equations of motion are solved by employing the adaptive Runge-Kutta-Fehlberg method, which allows for the discretization of the time interval of interest. The influence of initial position of ball with respect to cup centre on both maximum contact pressure and the corresponding ball trajectory of hip implants during a normal walking cycle are investigated. Moreover, the effects of clearance size, initial conditions and friction on the system dynamic response are analysed and discussed throughout this work.

2. Multibody dynamic model of the artificial hip joint

The multibody dynamic model originaly proposed by Askari et al. [16] has been considered here to address the problem of evaluating the contact pressure and moment of hip implants. A cross section *A-A* of a generic configuration of a hip joint is depicted in the diagram of in Fig. 1, which represents a total hip replacement. Figure 1 also shows the head and cup placed inside of the pelvis and separated from stem and neck. The forces developed along the interface of the ball and stem are considered to act in such a way that leads to a reaction moment, *M*. This moment can be determined by satisfying the angular motion of the ball centre during a walking cycle. The available data reported by Bergmann et al. [17] is used to define the forces that act at the ball centre. This data was experimentally obtained by employing a force transducer located inside the hip neck of a live patient. The information provided deals with the angular rotation and forces developed at the hip joint. Thus, the necessary angular velocities and accelerations can be obtained by time differentiating the angular rotation. Besides the 3D nature of the global motion of the hip joint, in the present work a simple 2D approach is presented, which takes into account the most significant hip action, i.e. the flexion-extension motion.

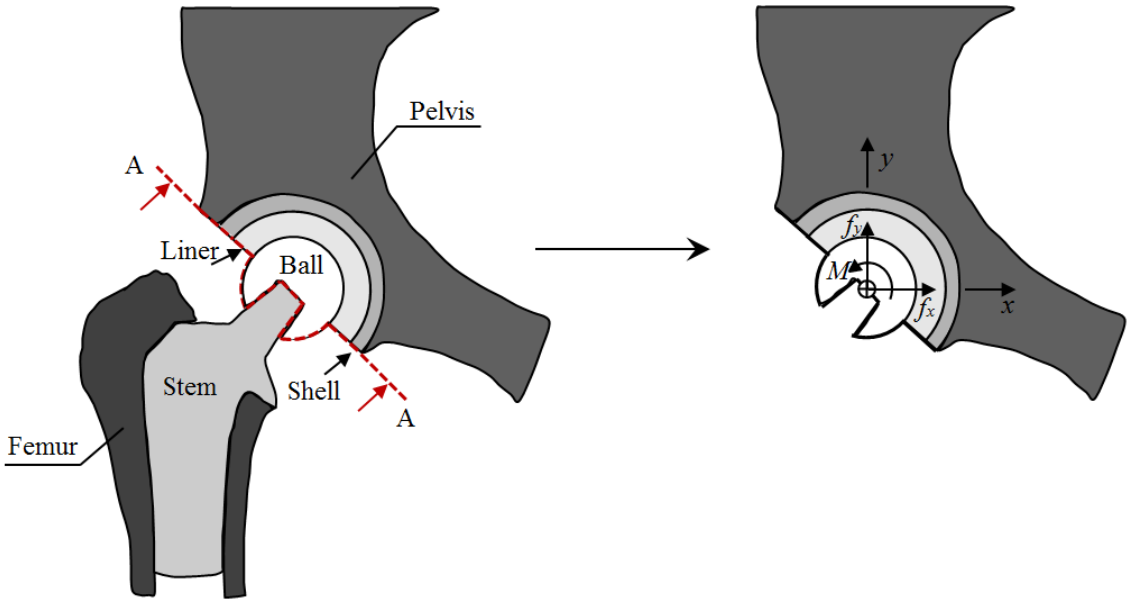

Fig. 1. A schematic of the artificial hip implant with the cross section *A-A* (Left figure), and the head and cup separated from the neck and stem through the cross section *A-A* (Right figure).

With regard to Fig. 2 the translational and rotational equation of motion of the head, for both free flight mode and contact mode, can be written by employing the Newton-Euler's equations [18, 19], yielding

$$\sum M_O \mathbf{k} = I\ddot{\theta}\mathbf{k}, \quad \sum \mathbf{M}_O = \begin{cases} Mk - \left(R_j\right) n \times \mathbf{F}_{P_j}^t & \delta > 0 \\ Mk & \delta \le 0 \end{cases} \tag{1}$$

$$\sum F_X = m\ddot{x}, \qquad \sum F_X = \begin{cases} f_x + (\mathbf{F}_{P_j}^t + \mathbf{F}_{P_j}^n) \cdot i & \delta > 0 \\ f_x & \delta \le 0 \end{cases} \tag{2}$$

$$\sum F_Y = m\ddot{y}, \qquad \sum F_Y = \begin{cases} f_y + \left(\mathbf{F}_{P_j}^n + \mathbf{F}_{P_j}^t\right) \cdot j - m & \delta > 0 \\ f_y & \delta \le 0 \end{cases} \tag{3}$$

where $\mathbf{F}_{P_j}^n$ and $\mathbf{F}_{P_j}^t$ denote the normal and tangential contact forces developed during the contact between the ball and cup, as it is represented in the diagram of Fig. 3. In Eqs. (1)-(3), x, y and θ are the generalised coordinates used to define the system's configuration. In turn, variable m and I are the mass and moment of inertia of ball, respectively. The external generalized forces are denoted by f_x, f_y and M and they act at the centre of the ball as it is shown in Fig. 3. The gravitational acceleration is represented by parameter g, R_j is the ball radius and δ represents relative penetration depth between the ball and cup surfaces.

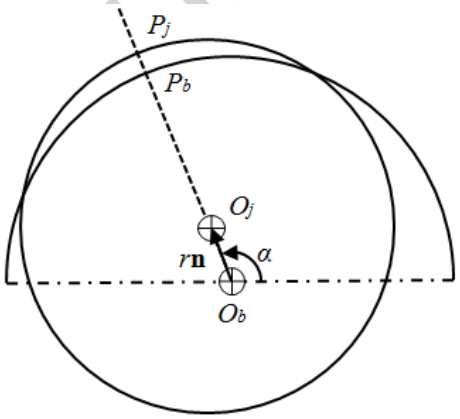

Fig. 2. A schematic of the head and cup interaction observed in the Sagittal plane.

The penetration depth can be expressed as [20]

$$\delta = r - (R_b - R_j) \tag{4}$$

in which R_b denotes the cup radius and (R_b-R_j) represents the joint radial clearance, which is a parameter specified by user.

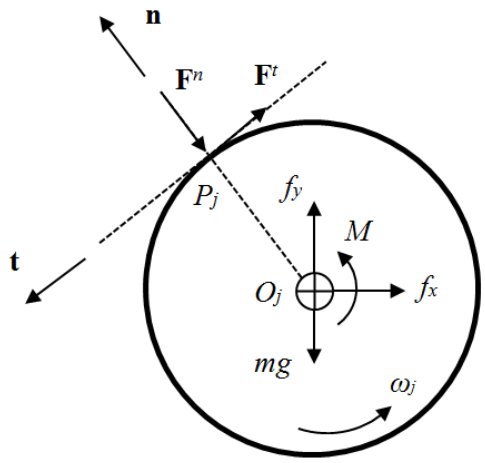

Fig. 3. Free body diagram of ball and corresponding external, internal and body forces and moment.

In the present study, the cup is assumed to be stationary, while the head describes the global motion. With regard to Fig. 2, it can be observed that O_j and O_b denote the head and cup centres, respectively. While P_j and P_b represent the contact points on the head and cup, respectively. The magnitude and orientation of the clearance vector are denoted by r and α, respectively. In general, r and α can be expressed as functions of the generalised coordinates used to describe the configuration of multibody mechanical system. The normal and tangential unit vectors at the contact point can be written as

$$\mathbf{n} = \cos\alpha\mathbf{i} + \sin\alpha\mathbf{j} \tag{5}$$

$$\mathbf{t} = -\sin\alpha\mathbf{i} + \cos\alpha\mathbf{j} \tag{6}$$

In order to compute the normal contact and tangential forces, it is first necessary to evaluate the relative tangential and normal velocities at the contact points, which can be obtained as follows [17]

$$\mathbf{v}_{p_j/p_b} = \dot{r}\,\mathbf{n} + \left(r\dot{\alpha} + R_j\omega_j\right)\mathbf{t} = v_n\mathbf{n} + v_t\mathbf{t} \tag{7}$$

where v_n and v_t are module of the normal and tangential velocities, respectively. Thus, Eqs. (2) and (3) can be re-written as follows

$$\begin{bmatrix} m & 0 \\ 0 & m \end{bmatrix} \begin{bmatrix} \ddot{x} \\ \ddot{y} \end{bmatrix} = \begin{bmatrix} \sum F_X \\ \sum F_Y \end{bmatrix} \tag{8}$$

Using now the concept of the state space representation, the second order equations of motion (8), can be expressed as a first order equation set as

$$\dot{\mathbf{z}} = \mathbf{H}(\mathbf{z}) \tag{9}$$

where $\mathbf{z} = \begin{bmatrix} z_1 \\ z_2 \\ z_3 \\ z_4 \end{bmatrix} = \begin{bmatrix} x \\ y \\ \dot{x} \\ \dot{y} \end{bmatrix}$ and $\mathbf{H}(\mathbf{z})$ is expressed as follows

$$\dot{\mathbf{z}} = \begin{bmatrix} \dot{z}_1 \\ \dot{z}_2 \\ \dot{z}_3 \\ \dot{z}_4 \end{bmatrix} = \begin{bmatrix} z_3 \\ z_4 \\ \sum F_X(\mathbf{z}) \\ \sum F_Y(\mathbf{z}) \end{bmatrix} \tag{10}$$

It must be mentioned that the r, α and their time derivatives can be obtained with respect to state space parameters as follows

$$\alpha = \text{atan}\left(\frac{z_2}{z_1}\right) \tag{11}$$

$$r = \sqrt{z_1^2 + z_2^2} \tag{12}$$

$$\dot{\alpha} = \frac{-z_2 z_3 + z_1 z_4}{z_1^2 + z_2^2} z_1^2 \tag{13}$$

$$\dot{r} = \frac{z_1 z_3 + z_2 z_4}{\sqrt{z_1^2 + z_2^2}} \tag{14}$$

It is known that the evaluation of the contact forces developed during an impact event plays a crucial role in the dynamic analysis of mechanical systems [21-23]. The contact forces must be computed by using a suitable constitutive law that takes into account material properties of the contacting bodies, the geometric characteristics of impacting surfaces and impact velocity. Additionally, the numerical approach for the calculation of the contact forces should be stable in order to allow for the integration of the mechanical systems equations of motion [24]. Different constitutive laws are suggested in the literature, being one of the more prominent proposed by Hertz [25]. However, this law is purely elastic in nature and cannot explain the energy loss during the impact process. Thus, Lankarani and Nikravesh [26] overcame this difficulty by separating the contact force into elastic and dissipative components as

$$\mathbf{F}_{p_j}^n = \left(K\delta^n + D\dot{\delta}\right)\mathbf{n} \tag{15}$$

Regarding Lankarani and Nikravesh model, normal contact force on the head is expressed as

$$\mathbf{F}_{p_j}^{n} = -K\delta^{\frac{3}{2}}\left(1+\frac{3\left(1-c_e^2\right)}{4}\frac{\dot{\delta}}{\dot{\delta}^{(-)}}\right)\mathbf{n} \tag{16}$$

where $\dot{\delta}$ and $\dot{\delta}^{(-)}$ are the relative penetration velocity and the initial impact velocity, respectively, and c_e is the coefficient of restitution. The generalised stiffness parameter K depends on the geometry and physical properties of the contacting surfaces, which for two internal spherical contacting bodies with radii R_i and R_j can be expressed as [25]

$$K = \frac{4}{3(\sigma_i+\sigma_j)}\left(\frac{R_i R_j}{R_i - R_j}\right)^2 \tag{17}$$

in which the material properties σ_i and σ_j are given by

$$\sigma_z = \frac{1-\upsilon_z^2}{E_z} \tag{18}$$

At this stage, it must be said the use of Eq. (15) is limited by Love's criterion, that is, it is only valid for impact velocities lower than the propagation velocity of elastic waves across the solids [27].

It is known that the way in which the friction phenomena are modelled, plays a key role in the systems behaviour [28]. In the present study, the tangential friction force are evaluated by using a modified Coulomb friction law, which can be expressed as [29, 30]

$$\mathbf{F}_{p_j}^{t} = -\mu(v_t)\mathbf{F}_{p_j}^{n}\frac{v_t}{|v_t|}\mathbf{t} \tag{19}$$

The friction force is described in the sense of Coulomb's approach, and is proportional to the magnitude of the normal force developed at the contact points, where the ratio is the coefficient of friction, μ, which is dependent on the relative tangential velocity. The model considered in reference [17] is employed here for the purpose of evaluating the coefficient of friction, which can be written as

$$\mu(v_t) = \begin{cases} \left(-\frac{c_f}{{v_0}^2}\left(|v_t|-v_0\right)^2 + c_f\right)(v_t), & |v_t| < v_0 \\ \left(c_d + \left(c_f - c_d\right)\exp\left(-\xi\left(|v_t|-v_0\right)\right)\right)sgn(v_t), & |v_t| \geq v_0 \end{cases} \tag{20}$$

where ξ is a slop parameter. The first part of friction coefficient function is exhibits a continuous behaviour when the function is close to zero, in order to avoid the numerical instabilities associated with null tangential velocity. Figure 4 shows the plot of Eq. (20), which represents the Stribeck effect. Thus, it can be stated that with this approach, the stick/slip effect can be taken into account. In fact, the model can represent the dry friction behaviour and address stick/slip phenomenon in relative low velocity case accurately. Moreover, this modified Coulomb's friction model can avoid computational instability associated with the change of velocity direction.

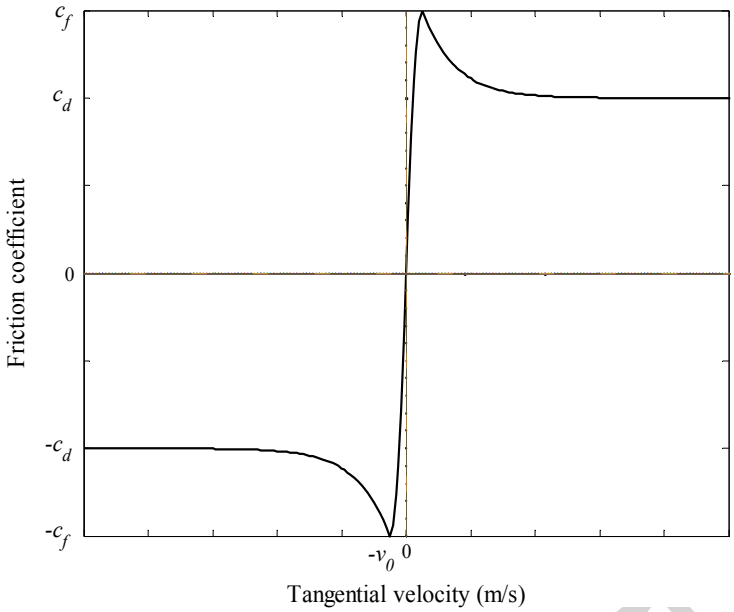

Fig. 4. Stribeck characteristic for dry friction.

Normal and tangential forces described above are present if the system is in contact situation, which means detecting impact or contact is one important step. Moreover, to compute the contact force, the initial impact velocity has to be calculated as an initial condition for following regimes, which could be in contact or in free flight, the following condition should be checked during the solution process by progressing time. Therefore, a contact event is detected when the following condition is verified

$$\delta\left(t^i\right)<0,\ \ \delta\left(t^{i+1}\right)>0 \tag{21}$$

Indeed, the precise instant in which the phase changes from free flight to contact is of paramount important instant because initial conditions for the next dynamic scenario are provided from exactly this instant [31].

3. Computing quasi-static and dynamic maximum contact pressures

For the CoC hip implants used nowadays, with 5, 3 and 2 mm thick ceramic insert, it has been demonstrated that the radius of the contact area between the femoral head and the acetabular cup is relatively small compared with that of the femoral head and the ceramic insert thickness. Therefore, the Hertzian contact theory can be utilised to estimate the contact parameters such as the maximum contact pressure and the contact area [1]. Hertzian contact theory can also be considered to evaluate contact pressures in CoC hip arthroplasty even though the ball is in contact with the cup as edge loading in CoC hip arthroplasty [5]. When the system is in edge-loading, the contact area is no longer circle but ellipse [4, 5]. In the present study, contact pressure and contact area are determined using two different approaches, namely quasi-statics and dynamics.

Assuming that the cup and head held in contact by a force F, as it is shown in Fig. 5, such that their point of contact expands into a circular area of radius a, [32]

$$a = K_a \sqrt[3]{F} \tag{22}$$

where

$$K_a = \left(\frac{3}{4} \frac{\frac{1-\upsilon_1^2}{E_1} + \frac{1-\upsilon_2^2}{E_2}}{\frac{1}{R_j} - \frac{1}{R_b}} \right)^{1/3} \tag{23}$$

in which υ_1, E_1 and υ_2, E_2 are Poisson's ratios and elastic modulii for the ball and cup, respectively. The maximum contact pressure occurs at the centre point of the contact area and can be calculated as

$$P_{max} = \frac{3F}{2\pi a^2} \tag{24}$$

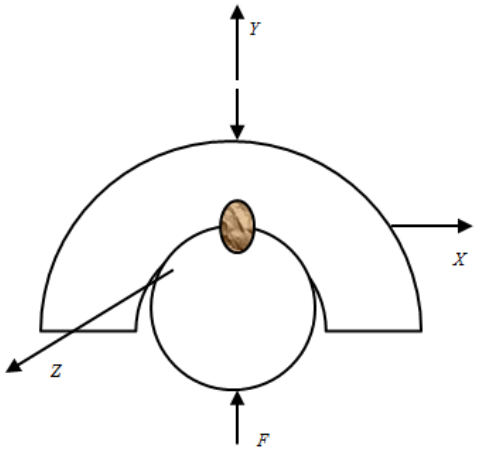

Fig. 5. Head and cup held in contact by a force *F*.

The local coordinate system (*XYZ*) is located at the centre point of the contact area as it is illustrated in Fig. 1. Since the coordinate system is defined as a local system, the tangential stresses can expressed as [32]

$$\sigma_{XZ} = -\mu(v_t) \frac{v_t}{|v_t|} \lim_{Y \to 0} \sigma_Y = P_{max} \mu(v_t) \frac{v_t}{|v_t|} \tag{25}$$

For an element close to the contact point, when *Y* approaches zero, the principal stresses are written as

$$\sigma_1 = -P_{max}, \qquad \sigma_2 = -P_{max}\left(\upsilon + 0.5 + \mu(v_t)\right) \qquad \sigma_3 = -P_{max}\left(\upsilon + 0.5 - \mu(\upsilon_t)\right) \tag{26}$$

If $\left(\upsilon + \mu(v_t)\right) > 0.5$ so that $\sigma_{max} = -P_{max}\left(\upsilon + 0.5 + \mu(v_t)\right)$ if $\left(\upsilon + \mu(v_t)\right) \le 0.5$ so that $\sigma_{max} = -P_{max}$.

Normal contact force, Eq. (16), is calculated as a function of time, solving resultant equations of multibody dynamic system. This normal contact force is substituted into Eqs. (22) and (24) to determine contact pressure distribution and contact area in ceramic-on-ceramic hip implants dynamically. To acquire quasi-static results, external normal contact loads (*F*) based on ISO14242-1

testing standard are introduced into Eqs. (22) and (24). These two approaches allows for the comparison between dynamic and quasi-static situations. Therefore, it is convenient to define a parameter, *dif.*, that conveys the difference between quasi-static and dynamic results of maximum contact pressures. Projection of the governing motion equations, Eq. (8), on the normal direction vector **n** provides the ball motion equation in normal direction as

$$m\ddot{\delta} = f_x cos\alpha + (f_y - mg)sin\alpha - F_{P_j}^n = f_{ext,n} - f_{cont,n} \tag{27}$$

where $\ddot{\delta}$ denotes the indentation acceleration. Substituting contact area from Eq. (22), normal contact force computed from Eq. (15) and normal contact force from ISO 14242-1 testing standard into Eq. (24), then, the difference between the cube of maximum contact pressures computed from quasi-static analysis and dynamic analysis can be evaluated as follows

$$\text{dif.} = \sigma_{max,qs}^3 - \sigma_{max,d}^3 = \frac{27}{8\pi^3 k_a^6} m\ddot{\delta} \tag{28}$$

The angular acceleration of femoral head can be calculated as the derivative of the ball angular velocity during a normal walking cycle. An external moment, *M*, which acts on the ball centre is required to cause hip implant to rotate with the known angular acceleration during a corresponding activity cycle. Therefore, the angular momentum, Eq. (1), has to be solved to obtain the external moment as follows

$$M\mathbf{k} = \begin{cases} I\ddot{\theta}k + \left(R_j\right)n \times \mathbf{F}_{P_j}^t & \delta > 0 \\ I\ddot{\theta}k & \delta \le 0 \end{cases} \tag{29}$$

4. Description of numerical model utilised

It is known that the resultant equations of multibody dynamic models for hip implants, Eq. (9), are nonlinear and must be solved by using numerical method. Thus, in the present work, an adaptive Runge-Kutta-Fehlberg method is considered to discretise the interval of time of analysis. An error threshold is defined. The error magnitude is calculated by comparing results obtained from explicit method with different orders. If the error magnitude is greater than the error threshold, the time step, *h*, must be halved and computation is done again in order to acquire accurate and stable outcomes. In the present study, the angular velocity around the flexion/extension direction *z*, ω_j, together with the force in the vertical direction, f_y, are considered. Vertical load and angular velocity are illustrated according to ISO14242-1 in Figs. 6 and 7, respectively. The geometrical and material properties of the head and cup are listed in Table 1. Moreover, integration step sizes for free flight and contact modes are assumed to be 0.00001s and 0.0000001s, respectively, being the corresponding integration tolerances 0.000001 and 0.00000001.

Table 1. Material and geometrical characteristics of the artificial hip joints.

Clearance size [mm]	0.05
Ceramic density [kg/m^3]	4370
Young modulus (cup-head) [GPa]	3.58e11
Poisson's ratio [-]	0.23
Restitution Coefficient [-]	0.9
Friction coefficients (C_f / C_d) [-]	0.15 / 0.1

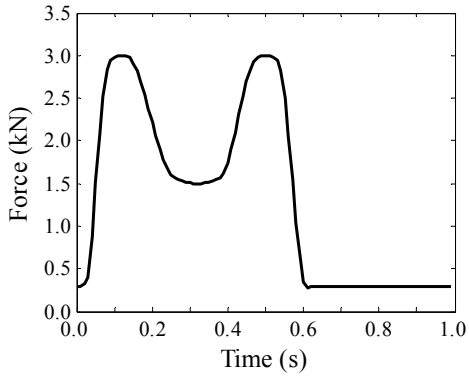

Fig. 6. The vertical load during a normal walking cycle based on ISO14242-1 testing standard [33, 34].

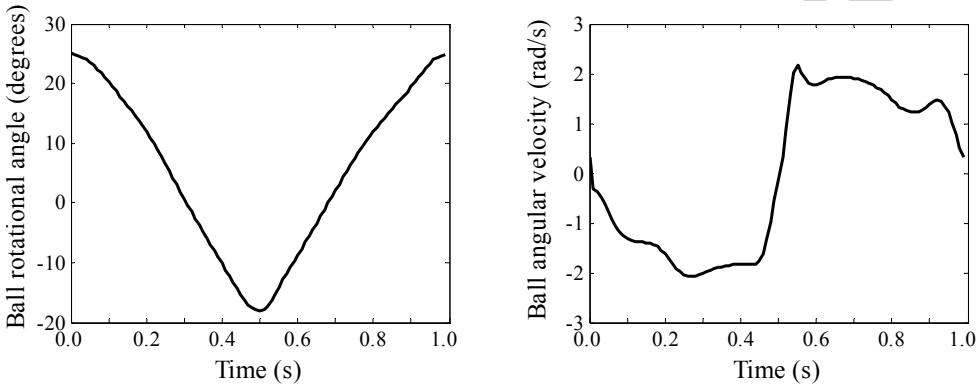

Fig. 7. (a) Rotation angle of ball; (b) The corresponding angular velocity based on ISO14242-1 testing standard.

5. Results and discussion

The comparison of maximum contact pressure and contact area outcomes between the multibody dynamic model and the quasi-static approaches are listed in Table 2. The data reported is for different radial clearances and cup radii, and it shows a good agreement between both methodologies. The data is relative to a cycle of 0.11 s, which corresponds to maximum external force, 3 kN, initial normal distance between head and cup is 0.0001 mm.

Table 2. Comparison of the predicted maximum contact pressure and contact area between the present multibody dynamic study and quasi-static approach.

Cup radius (mm)	Radial clearance (μm)	Maximum contact pressure (MPa)		Contact area (mm^2)	
		Multibody dynamic approach	Quasi-static approach	Multibody dynamic approach	Quasi-static approach
14	50	110.31	110.77	40.29	40.63
16	50	92.29	92.68	48.14	48.56
20	30	48.77	48.97	91.12	91.89
20	50	68.50	68.80	64.87	65.41
20	100	108.58	109.03	40.94	41.27
25	50	50.87	51.07	87.37	88.10

5.1 Effect of ball initial condition on hip implant maximum contact pressure and moment

The influence of the initial conditions on contact pressure developed in hip implants is depicted in Fig. 8. Initial ball position can be associated either with the separation of the head and cup at the start phase or with the likely start phase, in which fluid-film lubrication breaks down and the ball impacts the cup. The initial condition does not affect average magnitude of maximum contact pressure. The ball initiates its motion in free flight mode after bouncing several times from the cup surface and before the ball sits on the cup surface. It is obvious that when the system is in free flight mode, contact stress is zero. However, it increases suddenly and sharply when an impact between the cup and head takes place. It can also be observed that, the contact pressure exhibits an oscillating behaviour around its corresponding average contact pressure. The effect of free flight and impact modes on contact pressure is visible in the plots of Fig. 8c. It must be highlighted that initial impact velocity for Fig. 8c with initial position of (0, 0.02) is greater than Fig. 8a with initial position of (0, 0.0499). Consequently, as initial impact velocity rises, the contact force increases rapidly and the contact duration is shorter so that sitting the ball onto the cup takes longer as it can be observed in the plots of Figs. 8a and 8c. This result is in an agreement with the reference [35].

Ball with initial condition defined in Fig. 7d slides along the circumference of the cup and friction causes ball vibration to increase. This means that the ball in contact with the cup oscillates due to friction-induced vibration and stick/slip phenomenon notably [36, 37]. It leads to an oscillation behaviour of maximum contact pressure whose amplitude is comparable with the corresponding maximum contact stress. It must be said that these are the first results obtained on contact stresses in hip implants, taking friction-induced vibration, stick/slip friction and contact mechanics with standard hip joint forces during a normal walking cycle into account. Finally, the hip implant moment is evaluated for different initial conditions and the results are plotted in the diagrams of Fig. 9. It can be observed that the initial condition does not affect average magnitude of hip implant moment. Moreover, the head and cup are always in contact after the ball goes into the contact phase, although the ball center force is very low during the swing phase before ramping up at the heel-strike.

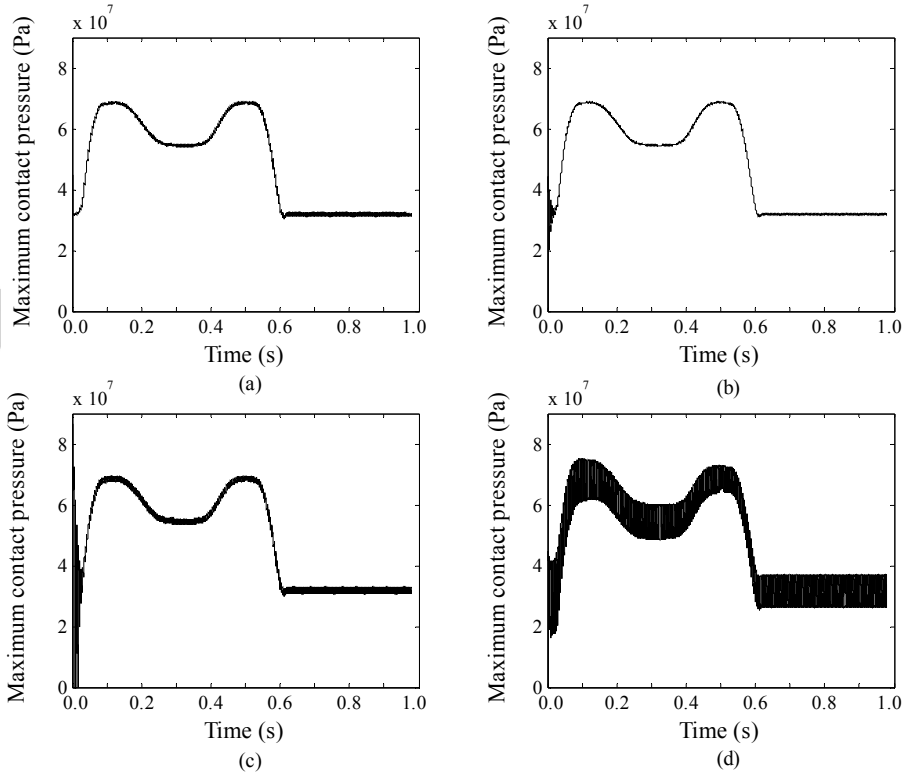

Fig. 8. The effect of ball initial conditions on maximum contact pressure during a normal walking cycle for different initial condition (mm): (a) (0, 0.0499); (b) (0.01, 0.0489); (c) (0, 0.02); (d) (0.0489, 0.01).

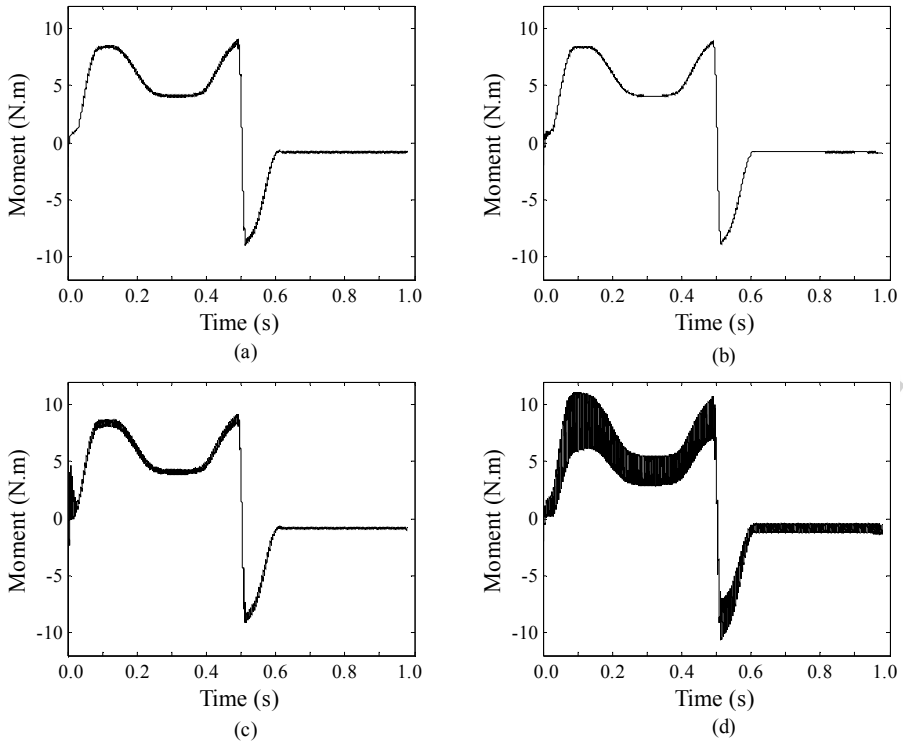

Fig. 9. The effect of ball initial conditions on maximum moment magnitude acting at the ball centre of hip implant during a normal walking cycle for different initial condition (mm): (a) (0, 0.0499); (b) (0.01, 0.0489); (c) (0, 0.02); (d) (0.0489, 0.01).

The ball centre trajectory inside the cup for initial condition (0.0489, 0.01) is depicted in Fig. 10a. It can be observed that the minimum and maximum angle of clearance vector are 11.56˚ and 168.57˚, respectively. It is of interest to determine not only how long the ball is in contact with the cup, but also what the corresponding average contact pressure is at each angle sub-interval defined above. The outcomes are depicted in Figs. 10c and 10d for cycle percentage and maximum average contact pressure versus clearance vector direction, respectively. This type of data can be considered to estimate tribological phenomena, such as wear caused by the relative sliding motion between the cup and head [38]. In addition, cube difference between maximum contact stresses computed from quasi-static and dynamic approaches can be obtained from Eq. (28), being the difference parameter *dif.* considered for comparative purpose. This parameter over a normal walking cycle is illustrated in Fig. 10b. As it can be seen, considerable differences are observed for the stance phase. The value of *dif.* is about constant in the swing phase. This discrepancy is due to the oscillating behaviour of the ball in contact with the cup since the vibration and dynamics of the ball due to friction-induced vibration, stick/slip phenomenon, angular speed changes and external force changes. A similar investigation is carried out and illustrated in the plots of Fig. 11 for a hip implant with initial condition (0, 0.0499). The corresponding minimum and maximum angle of clearance vector (α) are 75.22˚ and 103.08˚, respectively. It is worth noting that the femoral head is only about 1% of walking cycle, Fig. 11, within the vicinity of that sub-interval including the angle of 90˚ by virtue of friction and ball angular velocity. Differences between initial conditions of hip implant considered in Figs. 10 and 11 lead to different initial tangential impact velocity. Hence, the oscillating behaviour of the hip implant with initial condition (0.0489, 0.01) is greater than that with (0, 0.0499) due to friction-induced vibration and stick/slip phenomenon. Thus, it can be concluded that the effect of friction-induced vibration is

significant, especially when the tangential velocity of the ball due to its initial condition varies in a great enough range. Finally, the maximum contact stresses for $\alpha > 90^{\circ}$ are greater than those for $\alpha \leq 90^{\circ}$, as it can be observed in Fig. 11. In the last case, it can be explained that the angular velocity of the ball for the first half of the walking cycle, in which maximum external loads are acted on the ball centre, is negative so the ball slides along the cup surface in a counter-clockwise direction.

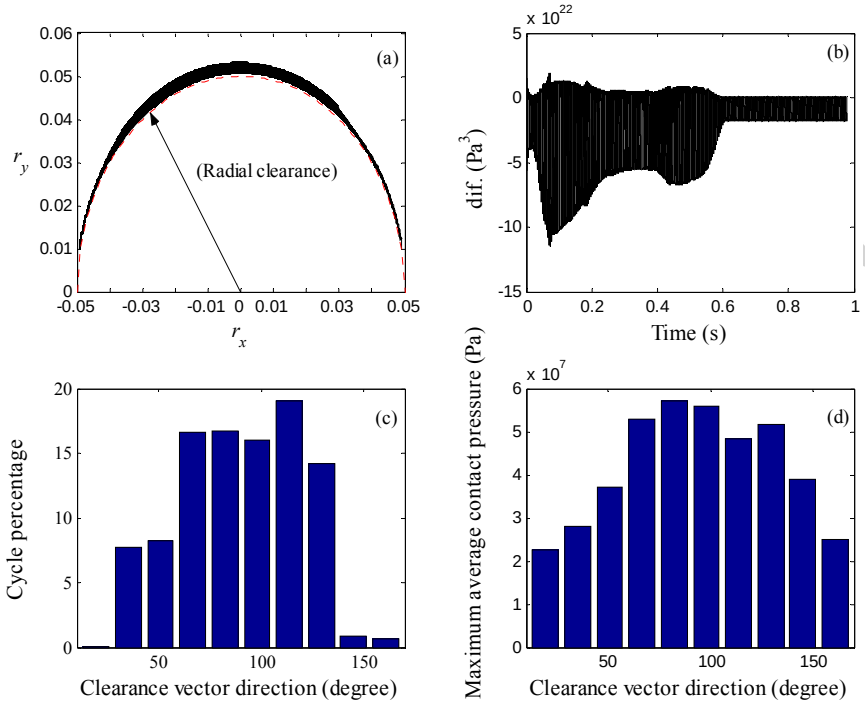

Fig. 10. (a) A representation of ball trajectory with respect to cup centre; (b) Difference between cube maximum contact pressure, *dif.*, Eq. (28); (c) The cycle percentage; (d) Average of maximum contact pressure. Cup radius: 20 mm and ball initial condition: (0.0489, 0.01).

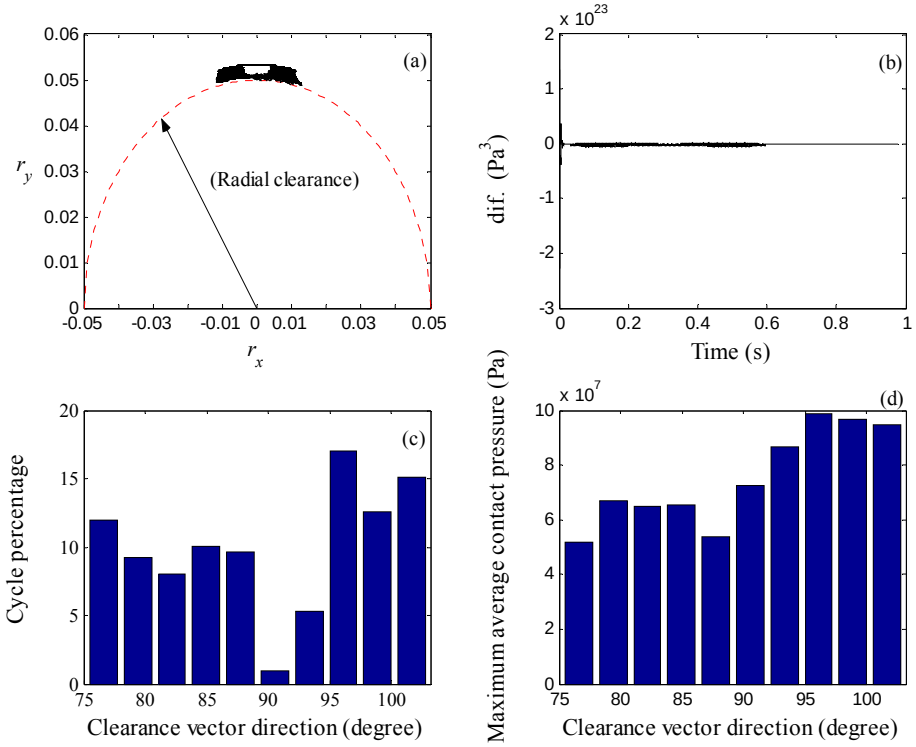

Fig. 11. (a) A representation of ball trajectory with respect to cup centre; (b) Difference between cube maximum contact pressure, *dif.*, Eq. (28); (c) The cycle percentage; (d) Average of maximum contact pressure. Cup radius: 14 mm and ball initial condition: (0, 0.0499).

5.2 Effect of friction on hip implant moment and maximum contact pressure

By analysing Eqs. (19) and (29), it can be observed that there is a linear relation between friction coefficient and hip implant moment. As it was expected, Fig. 12 shows that the friction has a considerable effect on hip implant moment. Hip implants with high friction experience greater moments, which can cause the prosthetic implant to loosen. Therefore, it can be sated that the friction-induced vibration and stick/slip friction could be a concern when the friction coefficient of contacting surfaces in artificial hip joint increases. It is observed that the decreasing ratio between hip implant moments and friction coefficients of hip implant in Fig. 12c and Fig. 12d is about similar, 1/1000. The effect of friction forces at the contact point on hip implant moment is dominant compared to the angular momentum of the femoral head, Eq. (19). This is concluded because the variation trend of moment in Fig. 12 is near external force's trend. The contact stresses are not affected notably by friction except for the oscillation trend of contact pressures. Moreover, comparing the plots of Figs. 12a and 12b it can be observed that during the first seconds of the walking cycle, the ball sits on the cup surface with higher friction case sooner than that with lower friction case. This means that more impacts followed by rebounds take place when friction is lower. Hence, in the case of lower friction, the possibility that fluid-film lubrication in artificial hip joints is built again, soon after the fluid film is ruptured and the ball impacts the cup surface, is more likely.

6. Conclusions

The hypothesis that friction-induced vibration and stick/slip friction can affect the contact pressure and the moment of artificial hip joints has been investigated throughout this paper. For this purpose, a multibody model was presented, which was validated and compared with a quasi-static approach. It was shown that friction-induced vibration can significantly affect contact pressure and moment in hip implants by importing an oscillating behaviour in the system dynamics. It must be stated that the proposed model is successful not only at taking friction-induced vibration, stick/slip phenomenon and contact/impact mechanics into account, but also at computing the pressure field at the contact zone

during different gait patterns. These features can be employed to gain a better understanding of tribological phenomena, such as wear caused by the relative sliding motion between the cup and head, onto contacting surfaces of the head and cup over time.

From the outcomes produced in this study, some relevant conclusions can be also drawn. Initial condition of the ball relative to the cup centre does not affect average magnitude of not only hip implant moment, but also contact stress. Moreover, a parameter, which showed difference between cube of maximum contact pressure, was defined and computed for different hip implant sizes and initial conditions. It was determined that oscillating behaviour of moment and contact stress plots was due to friction-induced vibration, stick/slip phenomenon, angular speed changes and ball centre force changes. It was also demonstrated that friction-induced vibration and stick/slip friction had a significant influence on the system dynamic response, because of negative gradient of friction coefficient, when tangential velocity of ball varied significantly. For a normal walking cycle, the cycle percentage in which the ball placed in different parts of cup inner surface was reported along with its corresponding average contact stress. The friction had also a considerable effect on hip implant moment, while contact stress average was not influenced by friction in a significant manner. Finally, future developments can be carried out in order to extend this research work to include other important issues, such as the lubrication phenomena [39, 40], elasticity of the contacting surfaces [41-43], as well as to validate the global results produced by comparing with experimental measurements [36].

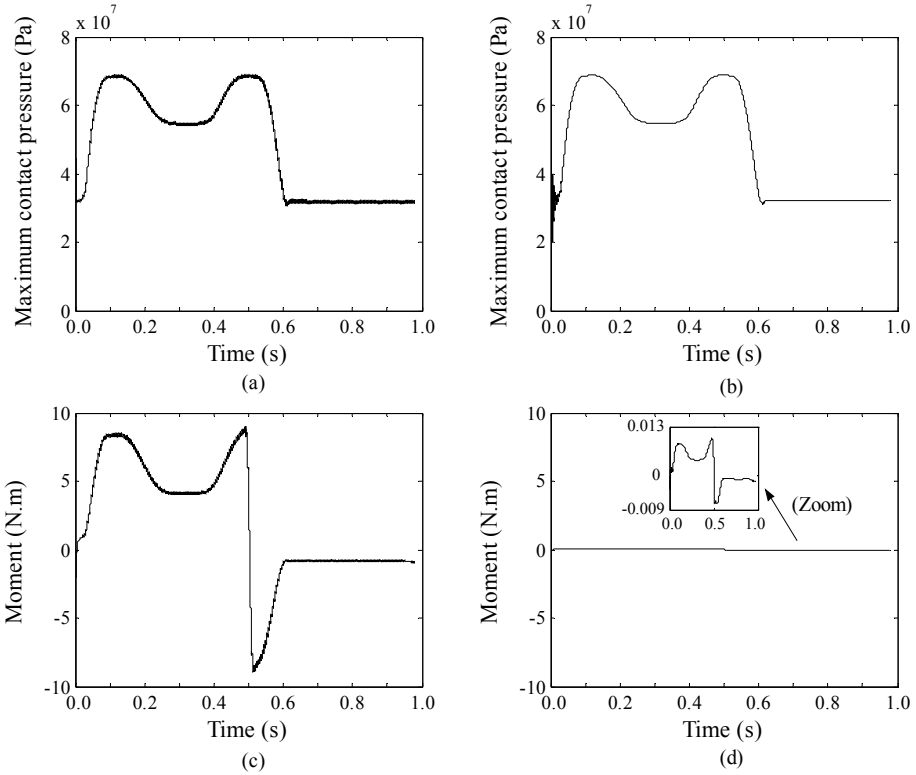

Fig. 12. Effect of friction on maximum contact pressure and moment of hip implant: (a) Maximum contact pressure with friction coefficient: 0.15 / 0.1; (b) Maximum contact pressure with friction coefficient: 0.00015 / 0.0001; (c) Hip implant ball moment with friction coefficient: 0.15 / 0.1; (d) Hip implant ball moment with friction coefficient: 0.00015 / 0.0001. Cup radius: 20 mm and initial condition: (0, 0.0499).

Acknowledgements

The first author gratefully acknowledges Macquarie University for International Macquarie University Research Excellence Scholarship (iMQRES) - No. 2010017. The second author expresses his gratitude to the Portuguese Foundation for the Science and Technology under the research project BIOJOINTS (PTDC/EME-PME/099764/2008).

References

[1] Mak M, Jin Z. Analysis of contact mechanics in ceramic-on-ceramic hip joint replacements. Proceedings of the Institution of Mechanical Engineers, Part H: Journal of Engineering in Medicine 2002;216(4):231-6.

[2] Meng Q, Liu F, Fisher J, Jin Z. Contact mechanics and lubrication analyses of ceramic-on-metal total hip replacements. Tribology International 2013;63:51-60.

[3] Mak M, Besong A, Jin Z, Fisher J. Effect of microseparation on contact mechanics in ceramic-on-ceramic hip joint replacements. Proceedings of the Institution of Mechanical Engineers, Part H: Journal of Engineering in Medicine 2002;216(6):403-8.

[4] Sariali E, Stewart T, Jin Z, Fisher J. Effect of cup abduction angle and head lateral microseparation on contact stresses in ceramic-on-ceramic total hip arthroplasty. Journal of Biomechanics 2012;45:390-393.

[5] Sanders A, Brannon R. Assessment of the applicability of the Hertzian contact theory to edge-loaded prosthetic hip bearings. Journal of Biomechanics 2011;44:2802-2808.

[6] Yoshida H, Faust A, Wilckens J, Kitagawa M, Fetto J, Chao E. Three-dimensional dynamic hip contact area and pressure distribution during activities of daily living. Journal of Biomechanics 2006;39:1996-2004.

[7] Bachtar F, Chen X, Hisada T. Finite element contact analysis of the hip joint. Medical and Biological Engineering and Computing 2006;44:643-651.

[8] Correa T, Crossley K, Kim H, Pandy M. Contributions of individual muscles to hip joint contact force in normal walking. Journal of Biomechanics 2010;43:1618-1622.

[9] Carriero A, Zavatsky A, Stebbins J, Theologis T, Lenaerts G, Jonkers I, Shefelbine S. Influence of altered gait patterns on the hip joint contact forces. Computer Methods in Biomechanics and Biomedical Engineering 2012:1-8.

[10] Zhu W, Puppulin L, Leto A, Takahashi Y, Sugano N, Pezzotti G. In situ measurements of local temperature and contact stress magnitude during wear of ceramic-on-ceramic hip joints Journal of the Mechanical Behavior of Biomedical Materials 2013, doi:10.1016/j.jmbbm.2013.01.018.

[11] Fialho J, Fernandes P, Eca L, Folgado J. Computational hip joint simulator for wear and heat generation. Journal of Biomechanics 2007;40:2358-2366.

[12] Uddin M, Zhang L. Predicting the wear of hard-on-hard hip joint prostheses. Wear 2013, doi:10.1016/j.wear.2013.01.009.

[13] Kim S, Lee S, Kang H, Jeong J. Study of knee and hip joints' moment estimation by biomechanical simulation during various motion changes. In: Proceedings of the world congress on engineering and computer science. San Francisco, USA: WCECS; 2009.

[14] Goldberg S, Stanhope S. Sensitivity of joint moments to changes in walking speed and body-weight-support are interdependent and vary across joints. Journal of Biomechanics 2013;46:1176-1183.

[15] Damm P, Ackermann R, Bender A, Graichen F, Bergmann G. In vivo measurements of the friction moment in total hip joint prostheses during walking. Journal of Biomechanics 2012;45:268.

[16] Askari E, Flores P, Turner D, Appleyard R. Planar multibody dynamic investigations of hip squeaking and ball trajectory in ceramic-on-ceramic artificial hip joints. In: VII Iberian Conference on Tribology. Porto, Portugal: FEUP; 2013.

[17] Bergmann G, Deuretzbacher G, Heller M, Graichen F, Rohlmann A, Strauss J, et al. Hip contact forces and gait patterns from routine activities. Journal of Biomechanics 2001;34(7):859-871.

[18] P.E. Nikravesh, Computer-aided analysis of mechanical systems, Prentice-Hall, Englewood Cliffs, New Jersey, 1988.

[19] Machado M, Flores P, Claro JCP, Ambrósio J, Silva M, Completo A, Lankarani HM. Development of a planar multi-body model of the human knee joint. Nonlinear Dynamics 2010;60(3):459-478.

[20] Flores P, Lankarani HM. Spatial rigid-multi-body systems with lubricated spherical clearance joints: modeling and simulation. Nonlinear Dynamics 2010;60(1-2):99-114.

[21] Silva PC, Silva MT, Martins JM. Evaluation of the contact forces developed in the lower limb/orthosis interface for comfort design. Multibody System Dynamics 2010;24:367-388.

[22] Lopes DS, Silva MT, Ambrósio JA, Flores P. A mathematical framework for contact detection between quadric and superquadric surfaces. Multibody System Dynamics 2010;24(3):255-280.

[23] Flores P, Machado M, Silva MT, Martins JM. On the continuous contact force models for soft materials in multibody dynamics. Multibody System Dynamics 2011;25(3):357-375.

[24] Machado M, Moreira P, Flores P, Lankarani HM. Compliant contact force models in multibody dynamics: evolution of the Hertz contact theory. Mechanism and Machine Theory 2012;53:99-121.

[25] Hertz H. Über die Berührung fester elastischer Körper. Journal reine und angewandte Mathematik 1881;92:156-171.

[26] Lankarani H, Nikravesh P. A contact force model with hysteresis damping for impact analysis of multibody systems. Journal of Mechanical Design 1990;112:369-376.

[27] Love A. A treatise on the mathematical theory of elasticity. 4th ed. New York: Dover; 1944.

[28] Muvengei O, Kihiu J, Ikua B. Numerical study of parametric effects on the dynamic response of planar multi-body systems with differently located frictionless revolute clearance joints. Mechanism and Machine Theory 2012;53:30-49.

[29] Hetzler H, Schwarzer D, Seemann W. Analytical investigation of steady-state stability and Hopf-bifurcations occurring in sliding friction oscillators with application to low-frequency disc brake noise. Communications in Nonlinear Science and Numerical Simulation 2007;12:83-99.

[30] Bai Z, Zhao Y, Chen, J. Dynamics analysis of planar mechanical system considering revolute clearance joint wear. Tribology International 2013;64:85-95.

[31] Flores P, Ambrósio J. On the contact detection for contact-impact analysis in multibody systems. Multibody System Dynamics 2010;24(1):103-122.

[32] Shigley J, Mischke C. Load and stress analysis, In Mechanical Engineering Design, 5th edition. New York: McGraw Hill; 1989.

[33] ISO 14242-1. Implants for surgery-wear of total hip-joint prostheses-part 1: loading and displacement parameters for wear-testing machines and corresponding environmental conditions for test, 2002.

[34] Rieker C, Schoen R, Liebentritt G, Gnepf P, Roberts P, Grigoris P. In-vitro tribology of large metal-on-metal implants-influence of the clearance. In: 50th Orthopedics Research Society, No. 123. San Francisco, California; 2004.

[35] Bai Z, Zhao Y. Hybrid contact force model of revolute joint with clearance for planar mechanical systems. International Journal of Non-Linear Mechanics 2013;48:15-36.

[36] Weiss C, Hothan A, Huber G, Morlock M, Hoffmann N. Friction-induced whirl vibration: Root cause of squeaking in total hip arthroplasty. Journal of Biomechanics 2012;45:297-303.

[37] Currier J, Anderson D, Van Citters D. A proposed mechanism for squeaking of ceramic-on-ceramic hips. Wear 2010;269:782-789.

[38] Flores P. Modeling and simulation of wear in revolute clearance joints in multibody systems. Mechanism and Machine Theory 2009;44:1211-1222.

[39] Flores P, Lankarani HM, Ambrósio J, Claro JCP. Modelling lubricated revolute joints in multibody mechanical systems. Proceedings of the Institution of Mechanical Engineers, Part-K Journal of Multi-body Dynamics 2004;218(4):183-190.

[40] Machado M, Flores P, Ambrósio J, Completo A. Influence of the contact model on the dynamic response of the human knee joint. Proceedings of the Institution of Mechanical Engineers, Part-K Journal of Multi-body Dynamics 2011;225(4):344-358.

[41] Tian Q, Zhang Y, Chen L, Flores P. Dynamics of spatial flexible multibody systems with clearance and lubricated spherical joints. Computers and Structures 2009;87:913-929.

[42] Tian Q, Sun Y, Liu C, Hu H, Flores P. Elastohydrodynamic lubricated cylindrical joints for rigid-flexible multibody dynamics. Computers and Structures 2013;114-115:106-120.

[43] Gao L, Yang P, Dymond I, Fisher J, Jin Z. Effect of surface texturing on the elastohydrodynamic lubrication analysis of metal-on-metal hip implants Tribology International 2010; 43:1851-1860.

Highlights:

- The effect of friction-induced vibration, stick/slip friction and contact/impact mechanics on maximum contact pressure and moment of artificial hip implants is investigated.
- A robust and easy-to-implement multibody dynamic model is performed.
- Friction has a considerable effect on hip implant moment.
- Friction-induced vibration and stick/slip friction affect contact pressure and moment in hip implants by importing an oscillating behavior in the system dynamics.

Graphical abstract

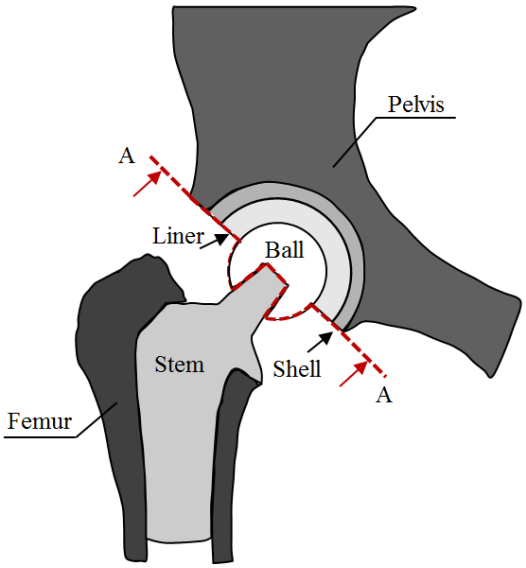

A schematic of the artificial hip joint with the cross section A-A.